Bioorganic Chemistry 89 (2019) 103026

Contents lists available at ScienceDirect

Bioorganic Chemistry

journal homepage: www.elsevier.com/locate/bioorg

Structural basis of the inhibition of GH1 β-glucosidases by multivalent pyrrolidine iminosugars

Macarena Martínez-Bailén[a], Elena Jiménez-Ortega[b], Ana T. Carmona[a], Inmaculada Robina[a], Julia Sanz-Aparicio[b,*], David Talens-Perales[c], Julio Polaina[c], Camilla Matassini[d], Francesca Cardona[d], Antonio J. Moreno-Vargas[a,*]

[a] Department of Organic Chemistry, Faculty of Chemistry, University of Seville, C/Prof. García González, 1, 41012 Seville, Spain
[b] Department of Crystallography and Structural Biology, Institute of Physical-Chemistry Rocasolano, CSIC, Serrano 119, 28006 Madrid, Spain
[c] Institute of Agricultural Chemistry and Food Technology, CSIC, 46980 Paterna, Valencia, Spain
[d] Department of Chemistry 'Ugo Schiff', University of Firenze, via della Lastruccia 3-13, 50019 Sesto Fiorentino (FI), Italy

ARTICLE INFO

Keywords:
Pyrrolidines
Iminosugars
Multivalency
β-glucosidase inhibitors
GH1 glycosidases
Klotho proteins

ABSTRACT

The synthesis of multivalent pyrrolidine iminosugars *via* CuAAC click reaction between different pyrrolidine-azide derivatives and tri- or hexavalent alkynyl scaffolds is reported. The new multimeric compounds, together with the monomeric reference, were evaluated as inhibitors against two homologous GH1 β-glucosidases (BglA and BglB from *Paenibacillus polymyxa*). The multivalent inhibitors containing an aromatic moiety in the linker between the pyrrolidine and the scaffold inhibited the octameric BglA (μM range) but did not show affinity against the monomeric BglB, despite the similarity between the active site of both enzymes. A modest multivalent effect (rp/n = 12) was detected for the hexavalent inhibitor **12**. Structural analysis of the complexes between the monomeric and the trimeric iminosugar inhibitors (**4** and **10**) and BglA showed the insertion of the inhibitors at the active site of BglA, confirming a competitive mode of inhibition as indicated by enzyme kinetics. Additionally, structural comparison of the BglA/**4** complex with the reported BglB/2F-glucose complex illustrates the key determinants responsible for the inhibitory effect and explains the reasons of the inhibition of BglA and the no inhibition of BglB. Potential inhibition of other β-glucosidases with therapeutic relevance is discussed under the light of these observations.

1. Introduction

β-Glucosidases are ubiquitous enzymes that play multiple biological roles and are present in all kind of living organisms. In bacteria and fungi, β-glucosidases are involved in the breakdown of cellulose and other carbohydrates [1]. In plants, these enzymes are involved in processes such as cell wall remodeling, chemical defense against pathogens and release of aroma components, among others [2]. In humans, β-glucosidases carry out the hydrolysis of glucosylceramide (GlcCer), which is in part performed by β-glucocerebrosidases GBA1 [3] and GBA2 [4]. A decreased activity of GBA1 is responsible for Gaucher disease [5], the most prevalent lysosomal storage disorder. Although GBA1 and GBA2 belong to the GH30 and GH116 families in the CAZy database [6], respectively, a large group of β-glucosidases belongs to the GH1 family. Members of this family are the well-studied sweet almond β-glucosidase [7,8] and the Klotho transmembrane proteins (α-Klotho, β-Klotho, and KL-related protein, KLrP). Deficiency of α-and β-Klotho proteins is a determinant factor in human aging [9,10,11]. Besides, it has been suggested that KLrP (formerly known as GBA3 or cytosolic β-glucocerebrosidase) is involved in the metabolic regulation of GlcCer through a novel catabolism pathway, although its exact function remains controversial [12]. Intestinal lactase phlorizin hydrolase (LPH), whose deficiency causes lactose intolerance [13] also belongs to GH1 family [14]. Bacterial enzymes are in general easy to manipulate and may serve as models to analyze structural problems related to homologous human proteins. In this respect, the two bacterial GH1 β-glucosidases A and B (BglA and BglB), isolated from the soil and plant-associated bacterium *Paenibacillus polymyxa* and involved in the hydrolysis of cellulosic substrates, could be useful models for GH1 enzymes. BglA is a cellobiase with an octameric quaternary structure [15],

* Corresponding authors at: Department of Organic Chemistry, Faculty of Chemistry, University of Seville, C/Prof. García González, 1, 41012 Seville, Spain (A.J. Moreno-Vargas); Department of Crystallography and Structural Biology, Institute of Physical-Chemistry Rocasolano, CSIC, Serrano 119, 28006 Madrid, Spain (J. Sanz-Aparicio).
E-mail addresses: xjulia@iqfr.csic.es (J. Sanz-Aparicio), ajmoreno@us.es (A.J. Moreno-Vargas).

https://doi.org/10.1016/j.bioorg.2019.103026
Received 2 May 2019; Received in revised form 24 May 2019; Accepted 30 May 2019
Available online 04 June 2019
0045-2068/

whereas BglB is a monomeric enzyme that acts as an exo-β-glucosidase hydrolyzing cellobiose and cellodextrins with higher degree of polymerization [16].

The interaction of multimeric inhibitors and glycosidases has been mostly explored in the case of Jack bean α-mannosidase as this enzyme has proven to be the most sensitive to multivalent binding [17,18,19,20,21,22]. Apart from Jack bean α-mannosidase, *N*-acetylgalactosamine-6-sulfatase (GALNS), a lysosomal enzyme deputed to the hydrolysis of glycosaminoglycans (GAGs) in the lysosomes, is likely to accept multivalent ligands [23,24]. Interestingly, both Jack bean α-mannosidase [25] and GALNS [26] have a dimeric structure. Although the mechanisms behind the observed multivalent effect have been studied with different indirect techniques, the interaction at the atomic level remains almost unexplored [27,28,29]. The greatest part of multivalent glycosidase inhibitors reported in the literature belongs to the six-membered iminosugar family (polyhydroxylated piperidines) [17–22], with only few examples of multivalent five-membered iminosugar (polyhydroxylated pyrrolidines) derivatives [29,30].

The elucidation of the chemical basis accounting for the interaction of inhibitors with GH1 glycosidases of therapeutic interest is the key issue to design selective inhibitors that could be useful to understand the exact function of these enzymes *in vivo*. Additionally, the potential application of the inhibitors as pharmacological chaperones (PCs) [31] to treat diseases caused by conformational deficiency of these enzymes could be of interest. PCs are molecules that bind with high specificity to a misfolded protein in the endoplasmic reticulum (ER), promoting the correct folding of the mutant protein. It has been observed that enzyme inhibitors can act as PCs at sub-inhibitory concentrations, with a correlation between the binding affinity and the chaperoning potency [32]. Regarding glycosidases, the chaperoning effect has been detected not only with small inhibitors but also with multivalent assemblies [33,34]. To achieve this goal, precise, atomic scale identification of the residues involved in protein-inhibitor interaction is required. Undoubtedly, X-ray crystallography analysis represents a unique tool for this purpose. Therefore, the objective of this work was to analyze the inhibition of GH1 β-glucosidases by mono- and multivalent pyrrolidine iminosugars (Fig. 1) by X-ray crystallography studies to gain detailed insight of the binding at the atomic level. The influence of structural parameters, such as the nature of the linker and valency of the multivalent compounds in the inhibition of model enzymes BglA and BglB has been analyzed. We chose these proteins as working models for GH1 glycosidases for three main reasons. Firstly, both enzymes have similar tertiary structure but a very different quaternary structure, BglA is an octamer whereas BglB is a monomer, that could be a determining factor in binding mono- or multivalent inhibitors. Secondly, BglA and BglB are suitable materials for crystallographic analysis at high resolution, as we have previously demonstrated [15,16]. Thirdly, our multivalent compounds are based on monomeric iminosugars that had previously shown inhibition towards other GH1 β-glucosidases (from almonds) [35]. In this manuscript we report the synthesis of new multivalent pyrrolidine derivatives (tri- and hexavalent), their inhibitory activity towards BglA and BglB and a precise, atomic resolution, description of the interactions responsible for the inhibition through X-ray crystallography.

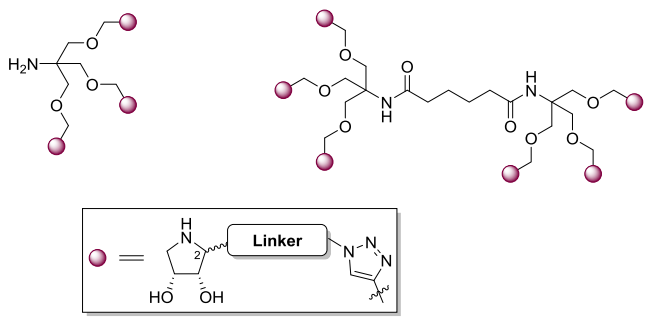

Fig. 1. Multivalent pyrrolidine iminosugars.

2. Results and discussion

2.1. Synthesis of the monovalent and multivalent inhibitors

For the synthesis of the multivalent compounds we used the Cu(I)-catalyzed azide-alkyne cycloaddition reaction (CuAAC) between tri- and hexavalent alkynyl scaffolds and pyrrolidine azides **3** and **6**, which were prepared from azidomethyl pyrrolidine **1**, in turn recently reported by our group [35]. CuAAC of **1** with aromatic alkyne **2** [36] (see Supporting Information) and subsequent treatment with NaN_3 afforded in excellent yield protected azide **3**, which after acidic deprotection gave unprotected derivative **4** (Scheme 1). Pyrrolidine azide **6** was prepared after CuAAC of **1** with alkyne **5** (see Supporting Information), nucleophilic displacement with NaN_3 and acidic deprotection.

The CuAAC reaction of azides **3** and **6** with the scaffolds **7** [37] and **8** (see Supporting Information for the synthesis of the alkynes) using $CuSO_4$ and sodium ascorbate in THF-H_2O and microwave irradiation at 80 °C afforded multivalent compounds **9–12** (Scheme 2). Due to the poor solubility of unprotected derivative **4** under CuAAC conditions, the click reactions were performed with the protected azido pyrrolidine **3**. The completion of the reaction was checked by ^{1}H NMR spectra of the crude mixtures, showing the disappearance of the signal at 2.42–2.44 ppm assigned to the terminal alkyne protons.

2.2. Biological evaluation

The inhibitory activities of compounds **9–12** towards BglA and BglB glucosidases were evaluated. Compounds **9** and **11** did not inhibit any of the enzymes while derivatives **10** and **12** showed competitive inhibition towards BglA in the micromolar range and no inhibition of BglB (Table 1), which is quite surprising considering the homology of both enzymes. These results point out the importance of the aromatic moiety of compounds **10** and **12** in the inhibition of BglA. In order to evaluate the existence of a multivalent effect, the valence-corrected relative inhibition potency (rp/n) was determined ($rp = K_{i\ (monov)}/K_{i\ (multiv)}$, n = valency of the cluster). A positive multivalent effect is observed when $rp/n > 1$ [19]. Pyrrolidine azide **4**, which was used as monovalent reference compound, showed a moderate competitive inhibition of BglA (K_i = 51 μM). Trivalent compound **10** and hexavalent **12** showed rp/n values of 2 and 12, respectively.

2.3. Structural insights into pyrrolidine iminosugar inhibition of BglA

The crystal structures of the BglA complexes with the inhibitors **4** and **10** have been solved to 2.1 and 2.8 Å resolution, respectively. Unfortunately, determination of co-crystal structures for **12** was unsuccessful. In both complexes, the asymmetric unit (a.u.) contains two subunits, A and B, of the functional octamer that are essentially identical and, therefore, the discussion will be focused on molecule A. The electron density obtained from both complexes shown in Fig. 2 allows unambiguous positioning of the inhibitors at the active site of BglA, with the pyrrolidine ring interacting with the catalytic residues, which confirms the competitive inhibition mode of the enzyme, as previously outlined by enzyme kinetics data. The only portion of the ligand presenting poor density is the distal part of the extended chain, i.e. the azidomethylene group of **4**, as this flexible segment lacks direct atomic interactions with residues at the active site that would stabilize a fixed conformation.

The precise recognition of **4** by BglA is given in Fig. 3a. The pyrrolidine ring occupies subsite −1 with its two hydroxyl groups mimicking the observed positions of O3 and O4 from the covalently bound glucose in the reported complex BglA-glucose (PDBV code 1E4I). Thus, the same net of hydrogen links is established with Gln20, Glu405 and

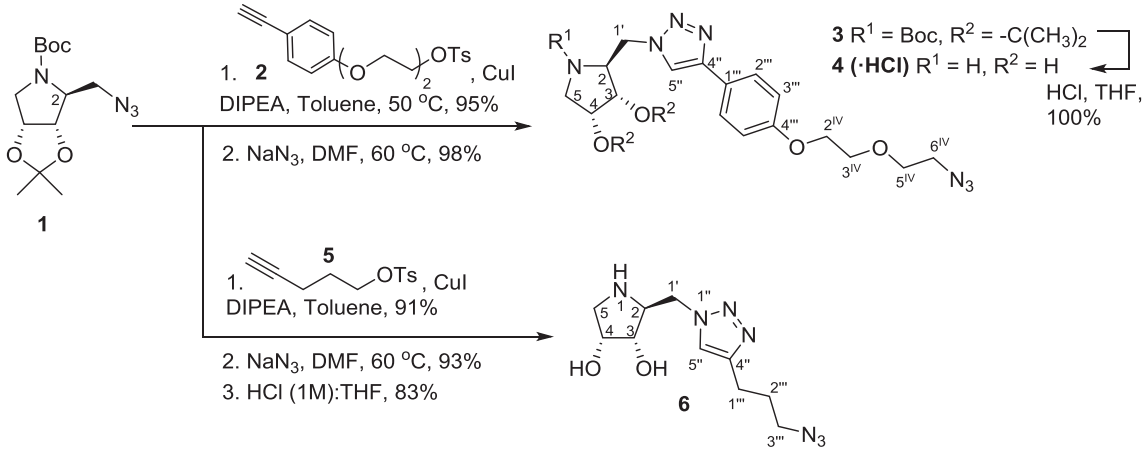

Scheme 1. Synthesis of the monovalent azidomethyl pyrrolidines.

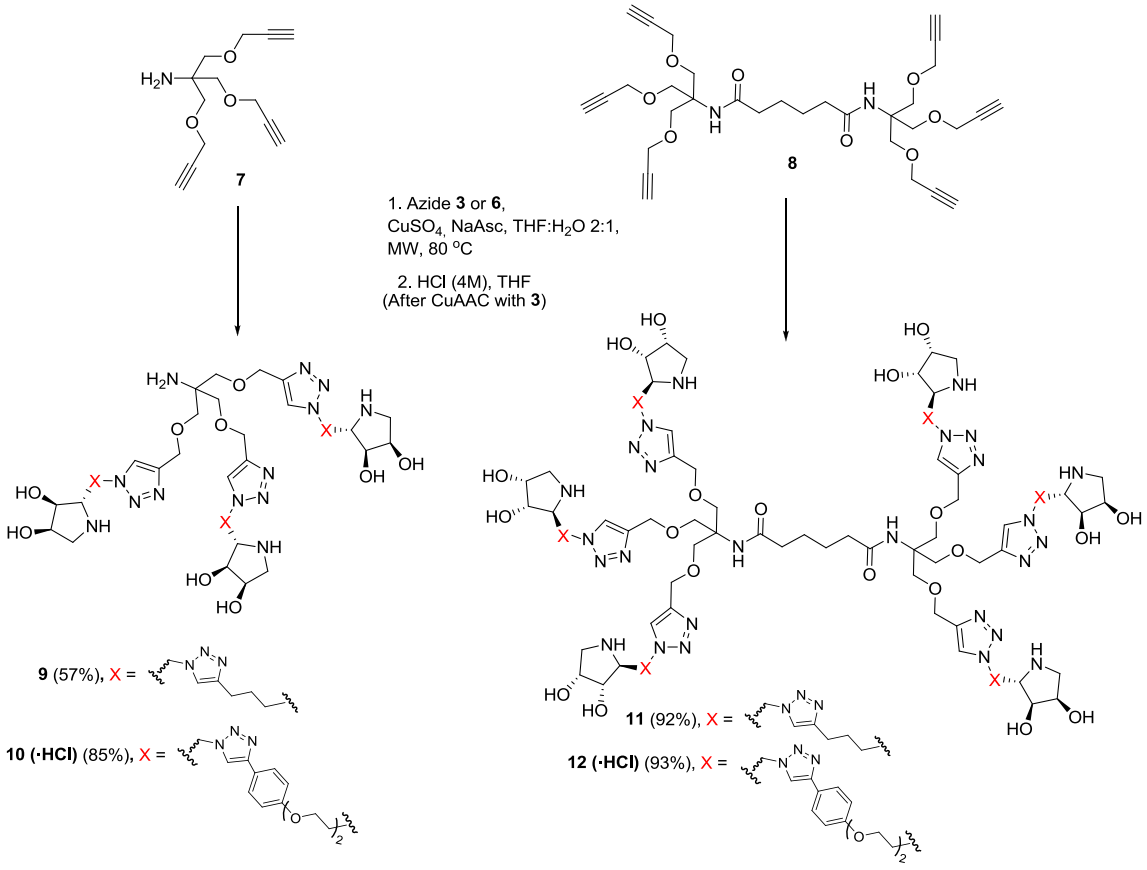

Scheme 2. Synthesis of multivalent compounds.

Trp406. Also, the endocyclic NH is hydrogen bonded to the carboxylates from Glu166/Glu352 and, altogether, this fixes the pyrrolidine in a tight position, which superimposes with the anomeric carbon of the glucose, as it has been observed previously in other GH1 complexes [38]. Moreover, the triazole, the phenyl ring and the C—C—O segment are accommodated through strong hydrophobic interaction with the residues shaping the narrow slit that gives access to the catalytic site. Thus, Trp326 in a *T*-mode interaction on one side, and Leu173, Leu177, Val179 and His180, on the opposite side, constrain an almost planar conformation of the ligand (see Fig. 3b). The fact that the tested ligands lacking the phenyl ring failed to inhibit BglA can be explained in terms of the higher ability of this group to adapt to the narrow slot, which confers a superior affinity of the ligands containing the phenyl moiety. On the contrary, the distal azidomethylene group protrudes from the cleft and is located in the channel that connects different subunits of the oligomer. Thus, as it can be seen in Fig. 3c and d, the BglA oligomer assembles the eight subunits with their corresponding active site faced in pairs, so that a 16–20 Å wide slit gives access to both cavities. All the subunits are occupied by an inhibitor molecule and, in this way, the distance between the terminal nitrogen atoms from each two bound ligand molecules is 12 Å (Fig. 3d).

In the solved structure of the BglA complexed with **10** (See Supplementary material), the absence of clear electron density, which vanishes from the ethylene glycol segment, as observed in Fig. 2b, precludes determining if the pyrrolidine moieties observed in the eight subunits come from the same or from two different trimer molecules

Table 1
IC_{50} (μM), K_i (μM) and rp/n for compounds **4**, **9–12**.

Structure	Compound (Valency, n)	BglA (rp/n)	BglB
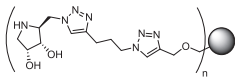	**9** (n = 3) **11** (n = 6)	–	–
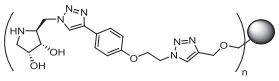	**10** (n = 3)	IC_{50} = 12, K_i = 8.5[a] (rp/n = 2.0)[b]	–
	12 (n = 6)	IC_{50} = 0.54, K_i = 0.72[a] (rp/n = 12)[b]	–
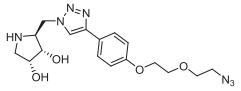	**4**	IC_{50} = 54, K_i = 51[a]	–

-: No inhibition was detected at 0.1 mM of compound.
[a] Competitive inhibition was observed by double Cornish-Bowden plots (See Supporting Information).
[b] rp = K_i (**4**)/K_i (multivalent).

(Figure S4 of Supplementary material). The premise of a same trimeric ligand entering the two confronted active sites is a feasible situation considering the topology of the octamer. However, also considering the flexibility of the ligand in the bridge segment and the absence of atomic interactions observed at this region with the enzyme, none of the alternative situations can be excluded. Consequently, the molecular mechanism of the multivalent effect remains elusive. The X-ray structure of BglA/**4** and BglA/**10** complexes showed a similar pattern of interaction with the enzyme and, in both cases, the inhibitor binds the active site of the enzyme. This fact discards the occlusion of this cavity by compound **10** through unspecific interactions outside the active site (Fig. 4c), which could be in agreement with the competitive inhibition found experimentally.

On the other hand, the multivalent effect observed for the hexamer is modest (rp/n = 12). This correlates much better with a statistical effect than with a chelate effect (Fig. 4a *vs* 4b) [39]. Nevertheless, the simultaneous interaction of trimer and hexamer with two or more enzymes (Fig. 4d) might not be discarded.

2.3.1. Molecular rationale of the inhibitory activity of pyrrolidine iminosugars vs GH1 enzymes

As it has been commented above, none of the tested compounds present inhibitory activity against BglB, despite this latter has appreciable similarities at the active site with respect to Bg1A. This observation can be rationalized on the basis of the corresponding three-dimensional structures. A structural superimposition of the BglA/**4** complex with the reported BglB/2F-glucose complex (PDB code 2JIE) [16] shows that the residues in both catalytic sites are well conserved (Fig. 5a). In this way, the phenyl moiety of the extrapolated position for a ligand molecule within the BglB active site could be allocated in the hydrophobic slit delineated by Trp328, in one side, and Tyr169, Leu174 and His181 in the opposite wall. However, some differences appear from distal positions that are more evident at the outer entrance to the cleft (Fig. 5b, c). Thus, the BglA residues Leu177, Val179, Ile324 and Glu408 are substituted by Thr178, Glu180, Met326 and Trp412 in BglB. In particular, and most remarkably, Glu180 protrudes at the BglB cleft probably producing deleterious clashes with the ligand, which may preclude the binding due to steric hindrance.

The same analysis may be performed to predict potential inhibition of other GH1 enzymes by these compounds. Thus, we have analyzed a possible effect on KLrP, a member of the Klotho family of proteins of known three-dimensional structure [40,41]. The structural superimposition of the KLrP/Glc complex (PDB code 2E9L) onto the BglA/**4** complex is shown in Fig. 6. As expected, the residues involved in recognition of the β-D-glucopyranose are conserved with the two described β-glucosidases, BglA and BglB, while the sequence divergence increases from the aglycon binding site. However, the orientation and the chemical nature of the BglA key residues Leu173, Val179, His180 and Glu408 are similar to the KLrP residues Met172, Met178, Phe179 and Gln427. Consequently, the phenyl ring of the inhibitor could be well allocated within a hydrophobic slit, stacked to Trp345 side-chain, and delineated by Met172, Leu176, Met178 and Phe179, therefore keeping the same interaction mode observed in the BglA/**4** and BglA/**10** complexes. This suggests that KLrP would also be inhibited. As the role of KLrP in the GlcCer metabolism *in vivo* is not defined yet [12], the development of selective inhibitors of this enzyme is important to elucidate the exact functions of the β-glucosidases involved in the metabolism of GlcCer and other glycosphingolipids.

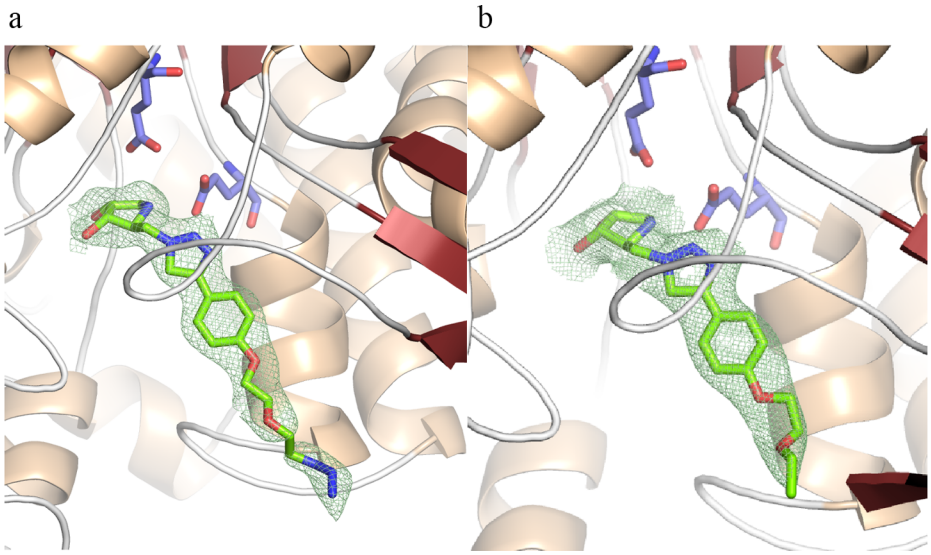

Fig. 2. Cartoon representation of BglA showing the molecules bound at its active site. Crystals soaked into compound **4** (a) and **10** (b). The catalytic residues are highlighted as blue sticks and the 2Fo-Fc electron density is contoured at 1.0 σ cut-off.

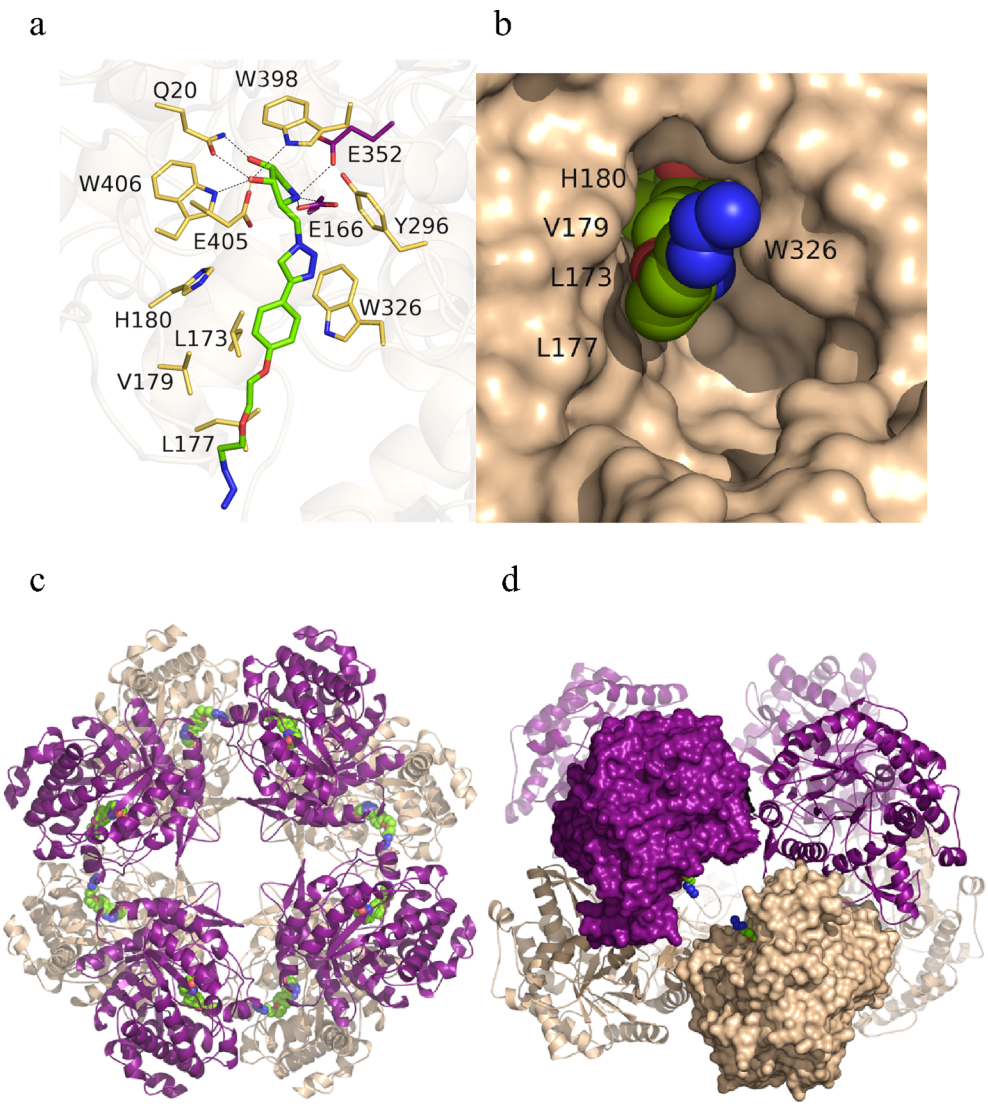

Fig. 3. Detail of the BglA active site in the crystals soaked into compound **4**. (a) Atomic interactions between the inhibitor (chartreuse) and relevant BglA residues (yellow) represented as sticks; the catalytic residues are highlighted in magenta and hydrogen bonds are represented with dashed lines. (b) Surface representation of BglA showing the narrow slot giving access to the catalytic pocket that is filled by the inhibitor; the hydrophobic residues shaping the slot are labelled. (c) and (d) Two perpendicular views of the BglA octamer, showing symmetry-related molecules A in beige and those corresponding to molecules B in magenta. In (d), the molecular surface of two subunits with faced active sites is represented, illustrating the relative position of each pair of bound inhibitor molecules existing in the octamer.

3. Conclusions

In summary, we have reported one of the very few examples of multivalent pyrrolidine derivatives with affinity against glycosidases, in this case a GH1 β-glucosidase. The multivalent compounds containing a phenyl moiety in the spacer between the pyrrolidine and the central scaffold selectively inhibited octameric GH1 β-glucosidase A from *P. polymyxa* (BglA), while no inhibition was detected against the homologous monomeric BglB. The structural analysis of the mono/trivalent inhibitors (**4** and **10**) in complex with BglA showed the pyrrolidine ring interacting with the catalytic residues in the active site, fixing the pyrrolidine in a tight position, which confirms the competitive inhibition mode of the enzyme. This analysis was crucial to explain both the exceptional selectivity of our inhibitors for BglA over homologous BglB and the requirement of a phenyl moiety in the arm spacer to achieve such inhibition. Although much more research is needed to understand the multivalent mechanisms operating in glycosidase inhibition, the structural analysis of the β-glucosidase inhibition by pyrrolidine iminosugars reported here will aid in the rational design of more potent and selective inhibitors of other GH1 glycosidases of therapeutic interest as KLrP.

4. Materials and methods

4.1. Chemistry

4.1.1. General methods

Optical rotations were measured in a 1.0 cm or 1.0 dm tube with a Jasco P-2000 spectropolarimeter. Infrared spectra were recorded with a Jasco FTIR-410 spectrophotometer. ^{1}H and ^{13}C NMR spectra were recorded with a Bruker Gemini 200, AMX300 and INOVA400 for solutions in $CDCl_3$, DMSO-d_6, CD_3OD and D_2O. δ are given in ppm and *J* in Hz. *J* are assigned and not repeated. All the assignments were confirmed by COSY and HSQC experiments. High resolution mass spectra were recorded on a Q-Exactive spectrometer. TLC was performed on silica gel 60 F_{254} (Merck), with detection by UV light charring with *p*-anisaldehyde, $KMnO_4$, ninhydrin or with Pancaldi reagent [$(NH_4)_6MoO_4$, $Ce(SO_4)_2$, H_2SO_4, H_2O]. Silica gel 60 (Merck, 40–60 and 63–200 μm) was used for preparative chromatography. Small scale microwave assisted syntheses were carried out in a CEM Discover or Anton Paar Monowave 300 microwave apparatus.

4.1.1.1. (2S,3S,4R)-N-tert-Butoxycarbonyl-2-[(4-(4-(2-(2-azidoethoxy) ethoxy)phenyl)-1H-1,2,3-triazol-1-yl)methyl]-3,4-O-isopropylidene-pyrrolidine-3,4-diol (3). To a solution of **1** [35] (925 mg, 3.10 mmol) in toluene

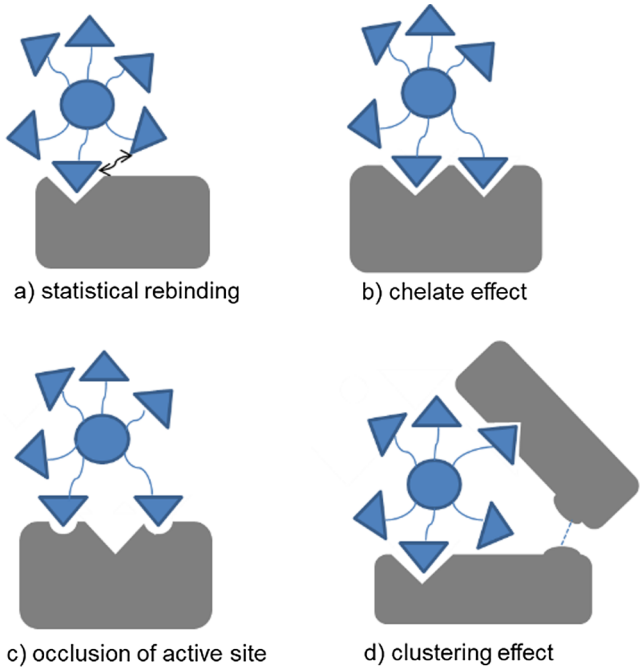

Fig. 4. Selected multivalent effects. (a) Statistical rebinding: the high local concentration of the inhitope may favour a recapture mechanism. (b) Chelate effect: simultaneous interaction of the inhibitor with two active sites of the enzyme. (c) Occlusion of active site: interactions of the inhibitor with non-catalytic subsites that block the active pocket. (d) Clustering effect: binding of the inhibitor to more than one enzyme at the same time.

(28 mL), alkyne **2** [36] (1.68 g, 4.66 mmol), DIPEA (2.1 mL, 12 mmol) and CuI (181 mg, 0.931 mmol) were added and the mixture was stirred at 50 °C for 30 h. Then, EtOAc and sat. aq. soln. of $NaHCO_3$ were added and the phases were separated. The aqueous phase was extracted with EtOAc (x2) and the combined organic layers were dried over Na_2SO_4, filtered and evaporated. Chromatographic purification on silica gel (EtOAc:cyclohexane 1:2→2:1) afforded the corresponding click derivative (1.93 g, 2.93 mmol, 95%) as a white solid. To a solution of this compound (1.93 g, 2.93 mmol) in DMF (25 mL), NaN_3 (482 mg, 7.34 mmol) was added. After stirring at 60 °C for 3 h the solvent was removed under vacuum and the crude product was dissolved in CH_2Cl_2, washed with water and brine, dried over Na_2SO_4, filtered and evaporated. The resulting residue was purified by chromatography column on silica gel (EtOAc:cyclohexane 1:1→2:1) to yield **3** (1.52 g, 2.87 mmol, 98%) as a grey solid. $[\alpha]_D^{29}$ + 26.8 (*c* 0.85, CH_2Cl_2). IR (ν cm^{-1}) 2981, 2935, 2100 (N_3), 1688 (C=O), 1498, 1402, 1246, 1123, 1056, 909, 729. ^{1}H NMR (300 MHz, DMSO-d_6, 363 K, δ ppm, *J* Hz) δ 8.29 (s, 1H, H-5″), 7.77–7.72 (m, 2H, H-aromat.), 7.05–7.01 (m, 2H, H-aromat.), 4.73–4.67 (m, 2H, H-3, H-4), 4.59 (dd, 1H, $^2J_{1'a,1'b}$ = 13.8, $J_{1'a,2}$ = 6.1, H-1′a), 4.44 (dd, 1H, $J_{1'b,2}$ = 7.0, H-1′b), 4.36–4.32 (m, 1H, H-2), 4.18 (t, 2H, $J_{H,H}$ = 4.8, H-2^{IV}), 3.82 (t, 2H, H-3^{IV}), 3.73–3.69 (m, 3H, H-5a, H-5^{IV}), 3.43 (t, 2H, $J_{H,H}$ = 5.0, H-6^{IV}), 3.20 (dd, 1H, $^2J_{5b,5a}$ = 12.9, $J_{5b,4}$ = 4.0, H-5b), 1.34 (s, 3H, -C(CH_3)$_2$), 1.31 (s, 9H, -C(CH_3)$_3$), 1.26 (s, 3H, -C(CH_3)$_2$). ^{13}C NMR (75.4 MHz, DMSO-d_6, 363 K, δ ppm) δ 158.0 (Cq aromat.), 153.1 (C=O, Boc), 146.0 (C-4″), 126.2 (C aromat.), 123.4 (Cq aromat.), 120.6 (C-5″), 114.7 (C aromat.), 110.6 (-*C*(CH$_3$)$_2$), 81.7 (C-3), 78.7 (-*C*(CH$_3$)$_3$), 78.4 (C-4), 68.9 (C-5^{IV}), 68.6 (C-3^{IV}), 67.2 (C-2^{IV}), 63.1 (C-2), 50.4 (C-5), 49.9 (C-6^{IV}), 48.6 (C-1′), 27.4 (-C(*C*H$_3$)$_3$), 26.3 (-C(*C*H$_3$)$_2$), 24.5 (-C(*C*H$_3$)$_2$). HRESIMS *m/z* found 530.2715, calc. for $C_{25}H_{36}N_7O_6$ [M + H]$^+$: 530.2722.

4.1.1.2. (2S,3S,4R)-2-[(4-(4-(2-(2-Azidoethoxy)ethoxy)phenyl)-1H-1,2,3-triazol-1-yl)methyl]-pyrrolidine-3,4-diol hydrochloride (4). A solution of **3** (55 mg, 0.10 mmol) in HCl (1 M):THF 1:1 (3.8 mL), was stirred at r.t. overnight. Evaporation of the solvent afforded **4** (47 mg, 0.10 mmol, quantitative) as a white solid. $[\alpha]_D^{25}$ – 42.7 (*c* 0.54, MeOH). IR (ν cm^{-1}) 3323, 3099 (OH, NH), 2911, 2100 (N_3), 1617, 1499, 1248, 1130, 1053, 828. ^{1}H NMR (300 MHz, CD_3OD, δ ppm, *J* Hz) δ 8.65 (s, 1H, H-5″), 7.77 (d, 2H, $J_{H,H}$ = 8.7, H-aromat.), 7.08 (d, 2H, H-aromat.), 5.12–5.01 (m, 2H, H-1′), 4.32–4.30 (m, 1H, H-4), 4.25–4.18 (m, 3H, H-3, H-2^{IV}), 4.13–4.06 (m, 1H, H-2), 3.89–3.86 (m, 2H, H-3^{IV}), 3.75 (t, 2H, $J_{H,H}$ = 4.9, H-5^{IV}), 3.62 (dd, 1H, $^2J_{5a,5b}$ = 12.6, $J_{5a,4}$ = 3.5, H-5a), 3.41–3.32 (m, 3H, H-6^{IV}, H-5b). ^{13}C NMR (75.4 MHz, CD_3OD, δ ppm) δ 161.4 (Cq aromat.), 147.7 (C-4″), 128.7 (C aromat.), 124.1 (C-5″), 121.6 (Cq aromat.), 116.4 (C aromat.), 74.8 (C-3), 71.3 (C-5^{IV}), 70.6 (C-3^{IV}), 70.3 (C-4), 68.9 (C-2^{IV}), 60.7 (C-2), 51.8 (C-6^{IV}), 51.7 (C-5), 51.3 (C-1′). HRESIMS *m/z* found 390.1876, calc. for $C_{17}H_{24}N_7O_4$ [M]$^+$: 390.1884.

4.1.1.3. (2S,3S,4R)-2-[(4-(3-Azidopropyl)-1H-1,2,3-triazol-1-yl)methyl]-pyrrolidine-3,4-diol (6). To a solution of **1** [35] (1.30 g, 4.36 mmol) in toluene (40 mL), alkyne **5** (1.55 g, 6.50 mmol), DIPEA (2.9 mL, 17 mmol) and CuI (253 mg, 1.30 mmol) were added and the mixture was stirred at r.t. for 1 d. Then, EtOAc and sat. aq. soln. of $NaHCO_3$ were added and the phases were separated. The aqueous phase was extracted with EtOAc (x2) and the combined organic layers were dried over Na_2SO_4, filtered and evaporated. Chromatographic purification on silica gel (EtOAc:cyclohexane 1:5→2:1) afforded the corresponding click derivative (2.12 g, 3.95 mmol, 91%) as a colourless oil. To a solution of this compound (1.99 g, 3.71 mmol) in DMF (32 mL), NaN_3 (607 mg, 9.24 mmol) was added. After stirring at 60 °C for 3 h the solvent was removed under vacuum and the crude product was dissolved in CH_2Cl_2, washed with water and brine, dried over Na_2SO_4, filtered and evaporated. The resulting residue was purified by chromatography column on silica gel (EtOAc:cyclohexane 1:1→2:1) to give the corresponding pyrrolidine-(azido)triazole (1.40 g, 3.44 mmol, 93%) as a yellow oil. A solution of this compound (492 mg, 1.21 mmol) in HCl (1 M):THF 1:1 (35 mL), was stirred at r.t. overnight. Evaporation of the solvent and chromatographic purification on Dowex 50WX8 eluting with MeOH, H_2O and NH_4OH 17%, afforded **6** (267 mg, 1.00 mmol, 83%) as a white solid. $[\alpha]_D^{29}$ – 45.2 (*c* 0.84, MeOH). IR (ν cm^{-1}) 3427, 3285 (OH, NH), 2097 (N_3), 1550, 1346, 1209, 979. ^{1}H NMR (300 MHz, CD_3OD, δ ppm, *J* Hz) δ 7.82 (s, 1H, H-5″), 4.60 (dd, 1H, $^2J_{1'a,1'b}$ = 14.0, $J_{1'a,2}$ = 4.1, H-1′a), 4.38 (dd, 1H, $J_{1'b,2}$ = 8.1, H-1′b), 4.02 (td, 1H, $J_{4,3}$ = $J_{4,5a}$ = 4.8, $J_{4,5b}$ = 3.0, H-4), 3.73 (dd, 1H, $J_{3,2}$ = 7.7, H-3), 3.47–3.41 (m, 1H, H-2), 3.36 (t, 2H, $J_{H,H}$ = 6.7, H-3‴), 3.12 (dd, 1H, $^2J_{5a,5b}$ = 12.0, H-5a), 2.87–2.76 (m, 3H, H-5b, H-1‴), 1.99–1.89 (m, 2H, H-2‴). ^{13}C NMR (75.4 MHz, CD_3OD, δ ppm) δ 147.8 (C-4″), 124.2 (C-5″), 76.2 (C-3), 72.3 (C-4), 62.7 (C-2), 53.9 (C-1′), 52.3 (C-5), 51.6 (C-3‴), 29.6 (C-2‴), 23.4 (C-1‴). HRESIMS *m/z* found 268.1518, calc. for $C_{10}H_{18}N_7O_2$ [M + H]$^+$: 268.1516.

4.1.2. General procedure for the synthesis of multivalent compounds:

To a solution of the protected or unprotected pyrrolidin-azide (3–6 eq) in THF:H_2O 2:1 (3 mL), were added $CuSO_4$ (0.3 eq per click reaction), sodium ascorbate (0.6 eq per click reaction) and the poly-propargylated scaffold (1 eq). The reaction mixture was heated in a MW reactor (80 °C, 0.75–3.0 h). After evaporation of the solvent, the resulting crude was purified by stirring with Quadrasil® MP followed by chromatography column (silica gel or Sephadex LH-20).

4.1.2.1. Polyhydroxylated trivalent iminosugar 9. CuAAC (*General procedure*) using **6** (54 mg, 0.20 mmol) and tripropargylated scaffold **7** [37] (16 mg, 0.068 mmol), afforded after 45 min of reaction and chromatographic purification (Sephadex LH-20, H_2O), compound **9** (40 mg, 0.039 mmol, 57%) as a pale yellow oil. $[\alpha]_D^{29}$ – 11.5 (*c* 0.67, H_2O). IR (ν cm^{-1}) 3269, 3138 (OH, NH), 2929, 1602, 1424, 1222, 1054, 813. ^{1}H NMR (400 MHz, D_2O, δ ppm, *J* Hz) δ 7.90–7.88 (m, 3H, H-5^{IV}), 7.69 (s, 3H, H-5″), 4.53 (dd, 3H, $^2J_{1'a,1'b}$ = 14.2, $J_{1'a,2}$ = 4.6, H-1′a), 4.48 (s, 6H, -OCH_2-triazole), 4.38–4.33 (m, 9H, H-1′b, H-3‴),

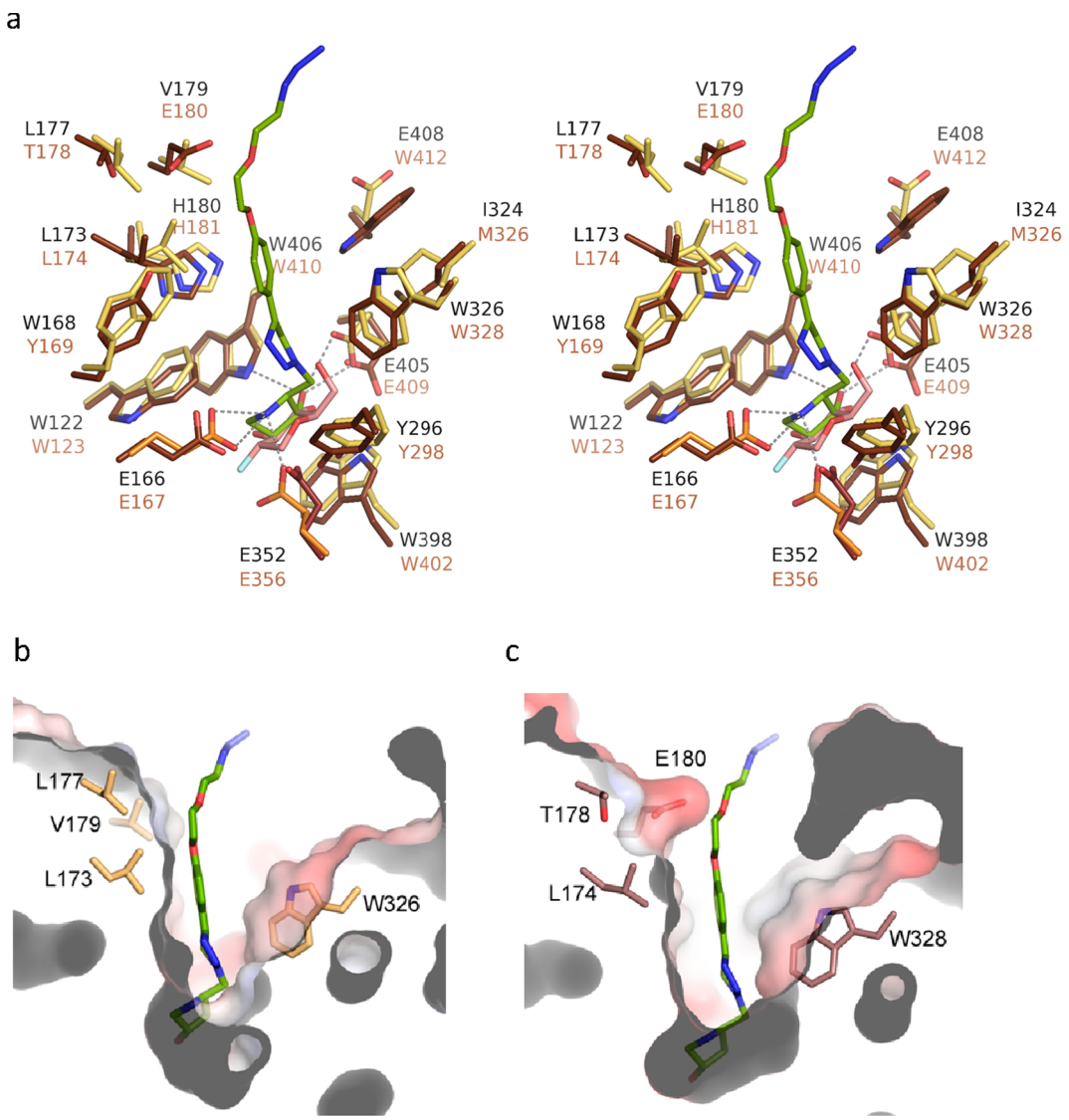

Fig. 5. Comparison of BglA and BglB active sites. (a) A stereo pair of the structural superimposition of the BglA/**4** (yellow) and BglB/2F-glucose (brown, PDB code 2JIE) complexes, showing the catalytic residues of BglA in orange and the ligand in chartreuse. The position of the ligand has been inferred in the BglB active site and the complex has been submitted to simple molecular dynamics. (b) A slice of the molecular surface of BglA with negative regions colored in red and relevant residues as sticks. (c) Same cross-section of the molecular surface of BglB. Glu180 protrudes into the catalytic channel and probably prevents binding of **4** to BglB.

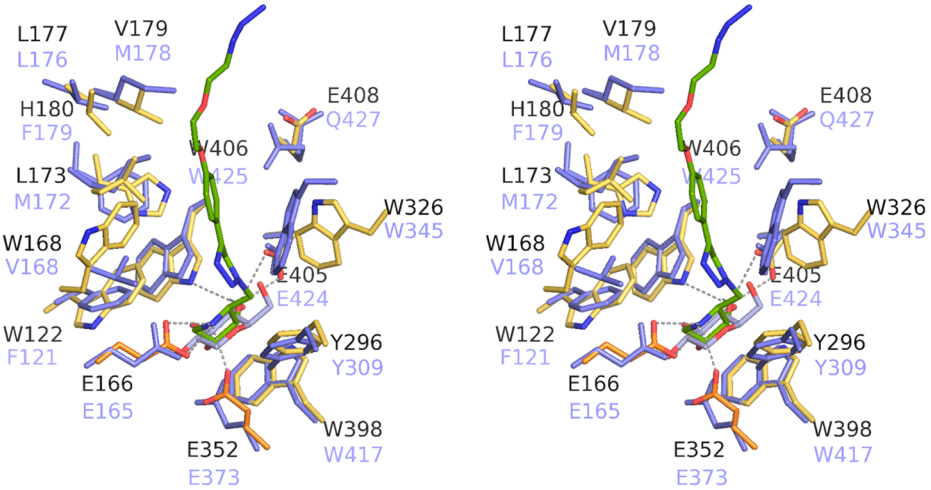

Fig. 6. Comparison of BglA and KLrP active sites. A stereo pair of the structural superimposition of the BglA/**4** (yellow) and KLrP/glucose (slate, PDB code 2E9L) complexes, showing the catalytic residues of BglA in orange and the ligand in chartreuse. The position of the ligand has been inferred in the KLrP active site and the complex has been submitted to simple molecular dynamics.

4.10–4.07 (m, 3H, H-4), 3.84–3.79 (m, 3H, H-3), 3.36 (br. s, 9H, H-2, H_2NCCH_2O), 3.10 (dd, 3H, $^2J_{5a,5b}$ = 12.6, $J_{5a,4}$ = 4.9, H-5a), 2.76 (dd, 3H, $J_{5b,4}$ = 2.5, H-5b), 2.59 (t, 6H, $J_{H,H}$ = 6.8, H-1‴), 2.17 (quint, 6H, $J_{H,H}$ = 6.7, H-2‴). ^{13}C NMR (50 MHz, D_2O, δ ppm) δ 146.6 (C-4″), 144.1 (C-4^{IV}), 124.9 (C-5^{IV}), 123.7 (C-5″), 74.6 (C-3), 70.9 (C-4), 70.5 (H_2NCCH_2O), 63.6 (−OCH_2-triazole), 60.7 (C-2), 52.6 (C-1′), 50.3 (C-5), 50.0 (H_2NCCH_2O), 49.6 (C-3‴), 28.8 (C-2‴), 21.6 (C-1‴). HRESIMS *m/z* found 1059.5419, calc. for $C_{43}H_{68}N_{22}O_9Na$ $[M + Na]^+$: 1059.5432.

4.1.2.2. Polyhydroxylated trivalent iminosugar 10·HCl. CuAAC (*General procedure*) using **3** (139 mg, 0.263 mmol) and tripropargylated scaffold **7** [37] (21 mg, 0.089 mmol), afforded after 1.5 h of reaction and chromatographic purification (silica gel, EtOAc:MeOH:NH_4OH 7:1:0.1→5:1:0.1), the corresponding protected trivalent iminosugar (138 mg, 0.0757 mmol, 85%) as a white solid. A solution of this compound (57 mg, 0.031 mmol) in HCl (4 M):THF (2:1, 4.5 mL) was stirred at r.t. for 4 h and evaporated to give **10·HCl** (54 mg, 0.031 mmol, quantitative) as a white solid. $[\alpha]_D^{24}$ – 29.3 (*c* 0.70, H_2O). IR (ν cm^{-1}) 3344, 3140, (OH, NH), 2925, 1616, 1511, 1254, 1111, 1053, 925, 838. ^{1}H NMR (300 MHz, D_2O, δ ppm, *J* Hz) δ 8.15 (s, 3H, H-5″), 7.87 (s, 3H, H-5^V), 7.39 (d, 6H, $J_{H,H}$ = 8.5, H-aromat.), 6.64 (d, 6H, H-aromat.), 4.84–4.81 (m, 6H, H-1′), 4.47–4.44 (m, 6H, H-6^{IV}), 4.34–4.30 (m, 9H, H-4, −OCH_2-triazole), 4.22 (dd, 3H, $J_{3,2}$ = 9.6, $J_{3,4}$ = 4.0, H-3), 4.03–3.95 (m, 3H, H-2), 3.84–3.78 (m, 12H, H-5^{IV}, H-2^{IV}), 3.61–3.54 (m, 9H, H-3^{IV}, H-5a), 3.37–3.33 (m, 9H, H-5b, H_2NCCH_2O). ^{13}C NMR (75.4 MHz, D_2O, δ ppm) δ 158.4 (Cq aromat.), 146.6 (C-4″), 142.6 (C-4^V), 127.1 (C aromat.), 125.6 (C-5^V), 122.2 (C-5″), 121.4 (Cq aromat.), 114.9 (C aromat.), 72.8 (C-3), 68.7 (C-4, C-3^{IV}), 68.4 (C-5^{IV}), 67.0 (H_2NCCH_2O), 67.0 (C-2^{IV}), 63.1 (-OCH_2-triazole), 59.0 (H_2NCCH_2O), 58.9 (C-2), 50.5 (C-6^{IV}), 50.1 (C-5), 49.1 (C-1′). HRESIMS *m/z* found 1403.6698, calc. for $C_{64}H_{87}N_{22}O_{15}$ $[M + H]^+$: 1403.6716.

4.1.2.3. Polyhydroxylated hexavalent iminosugar 11. CuAAC (*General procedure*) using **6** (61 mg, 0.23 mmol) and hexapropargylated scaffold **8** (22 mg, 0.038 mmol), afforded after 2 h and 15 min of reaction and chromatographic purification (Sephadex LH-20, H_2O), compound **11** (76 mg, 0.035 mmol, 92%) as a pale yellow oil. $[\alpha]_D^{29}$ – 19.4 (*c* 0.54, H_2O). IR (ν cm^{-1}) 3276, 3132 (OH, NH), 2929, 1649 (C=O), 1550, 1436, 1342, 1216, 1049, 823. ^{1}H NMR (400 MHz, D_2O, δ ppm, *J* Hz) δ 7.84 (s, 6H, H-5^{IV}), 7.69 (s, 6H, H-5″), 4.52 (dd, 6H, $^2J_{1'a,1'b}$ = 13.9, $J_{1'a,2}$ = 3.7, H-1′a), 4.43 (s, 12H, −OCH_2-triazole), 4.37–4.30 (m, 18H, H-1′b, H-3‴), 4.08 (br. s, 6H, H-4), 3.84–3.78 (m, 6H, H-3), 3.60 (s, 12H, −NHCCH_2O), 3.37 (br. s, 6H, H-2), 3.10–3.08 (m, 6H, H-5a), 2.76 (d, 6H, $^2J_{5b,5a}$ = 11.9, H-5b), 2.56 (t, 12H, $J_{H,H}$ = 6.8, H-1‴), 2.15–2.12 (m, 12H, H-2‴), 2.04 (br. s, 4H, −$CH_2C H_2$C = O), 1.36 (br. s, 4H, −CH_2CH_2C = O). ^{13}C NMR (50 MHz, D_2O, δ ppm) δ 176.1 (C=O), 146.6 (C-4″), 144.1 (C-4^{IV}), 124.8 (C-5^{IV}), 123.6 (C-5″), 74.6 (C-3), 70.9 (C-4), 67.6 (−NHCCH_2O), 63.6 (−OCH_2-triazole), 60.8 (C-2), 59.8 (−NHCCH_2O), 52.6 (C-1′), 50.3 (C-5), 49.6 (C-3‴), 35.9 (−CH_2CH_2C=O), 28.9 (C-2‴), 24.7 (−CH_2CH_2C=O), 21.7 (C-1‴). HRESIMS *m/z* found 1092.5787, calc. for ½($C_{92}H_{144}N_{44}O_{20}$) $[M + 2H]^{2+}$: 1092.5796.

4.1.2.4. Polyhydroxylated hexavalent iminosugar 12·HCl. CuAAC (*General procedure*) using **3** (113 mg, 0.213 mmol) and hexapropargylated scaffold **8** (21 mg, 0.036 mmol), afforded after 3 h of reaction and chromatographic purification (silica gel, EtOAc:MeOH:NH_4OH 5:1:0.1), the corresponding protected hexavalent iminosugar (126 mg, 0.0335 mmol, 93%) as a colourless oil. A solution of this compound (57 mg, 0.015 mmol) in HCl (4 M):THF (2:1, 2.1 mL) was stirred at r.t. for 4 h and evaporated to give **12·HCl** (55 mg, 0.015 mmol, quantitative) as a solid. $[\alpha]_D^{25}$ – 26.5 (*c* 0.53, H_2O). IR (ν cm^{-1}) 3328, 3140 (OH, NH), 2932, 1617 (C=O), 1511, 1257, 1186, 1106, 1053, 925, 837. ^{1}H NMR (300 MHz, D_2O, δ ppm, *J* Hz) δ 8.07 (s, 6H, H-5″), 7.77 (s, 6H, H-5^V), 7.29 (d, 12H, $J_{H,H}$ = 8.5, H-aromat.), 6.53 (d, 12H, H-aromat.), 4.79–4.75 (m, 12H, H-1′), 4.35–4.29 (m, 18H, H-6^{IV}, H-4), 4.20–4.16 (m, 18H, −OCH_2-triazole, H-3), 3.98–3.91 (m, 6H, H-2), 3.70–3.69 (m, 24H, H-5^{IV}, H-2^{IV}), 3.56–3.48 (m, 18H, H-5a, H-3^{IV}), 3.38–3.29 (m, 18H, −NHCCH_2O, H-5b), 1.85 (br. s, 4H, −$CH_2C H_2$C = O), 1.17 (br. s, 4H, −CH_2CH_2C = O). ^{13}C NMR (75.4 MHz, D_2O, δ ppm) δ 175.8 (C=O), 158.3 (Cq aromat.), 146.4 (C-4″), 142.9 (C-4^V), 126.9 (C aromat.), 125.5 (C-5^V), 122.1 (C-5″), 121.2 (Cq aromat.), 114.8 (C aromat.), 72.8 (C-3), 68.6 (C-4, C-3^{IV}), 68.4 (C-5^{IV}), 67.8 (−NHCCH_2O), 66.9 (C-2^{IV}), 62.9 (−OCH_2-triazole), 59.5 (−NHCCH_2O), 58.9 (C-2), 50.5 (C-6^{IV}), 50.1 (C-5), 49.1 (C-1′), 35.7 (−$CH_2C H_2$C = O), 24.5 (−CH_2CH_2C = O). HRESIMS *m/z* found 1469.6808, calc. for ½($C_{134}H_{179}N_{44}O_{32}Na$) $[M + H + Na]^{2+}$: 1469.6809.

4.2. Production and purification of BglA and BglB

His-tagged versions *Panibacillus polymyxa* β-glucosidases A and B with increased thermal stability were cloned in plasmid pQE80L vector (Stratagene). The enzymes were recovered from transformant *E. coli* cultures and purified by nickel affinity chromatography. The engineered versions of the two enzymes that were used contained the following mutations: BglA: E96K, T3855A, N411S, M416I and N437K [42], BglB: H62R, N223Y and M319I [43].

4.3. Inhibition studies with BglA and BglB

The % of inhibition towards the corresponding glycosidase (BglA or BglB) was determined in the presence of 0.1 mM of the inhibitor on the well. Each enzymatic assay (final volume 0.12 mL) contains 0.01–0.5 units/mL of the enzyme and 4.2 mM aqueous solution of the appropriate *p*-nitrophenyl β-D-glucopyranoside (substrate) buffered to the optimal pH of the enzyme (pH 6.5). Enzyme and inhibitor were pre-incubated for 5 min at rt, and the reaction started by addition of the substrate. After 20 min of incubation at 37 °C, the reaction was stopped by addition of 0.1 mL of sodium borate solution (pH 9.8). The *p*-nitrophenolate formed was measured by visible absorption spectroscopy at 405 nm. Under these conditions, the *p*-nitrophenolate released led to optical densities linear with both reaction time and concentration of the enzyme. The IC_{50} value (concentration of inhibitor required for 50% inhibition of enzyme activity) was determined from plots of % inhibition *versus* different inhibitor concentrations. For all the inhibitors, the mode of inhibition was suggested by the Dixon plot where reciprocal velocity (1/V) is plotted against concentration of inhibitor [I] at different substrate concentrations [S]. The intersection of lines gives K_i. The complementary Cornish-Bowden plot ([S]/V *versus* [I] at different substrate concentrations) was also represented to confirm the competitive inhibition mode [44]. The IC_{50} and K_i were determined by duplicate (< 10% of difference) and the average value is given.

4.4. Crystallization and structure determination of the BglA complexes.

The first attempts to obtain crystals from the reported crystallization conditions for wild type BglA were unproductive [14]. New crystallization conditions were explored by high-throughput techniques with a NanoDrop robot (Innovadyne Tecnhologies Inc.), using two commercial screens: Index (Hampton Research) and JBScreen PACT++ (Jena Bioscience). Preliminary bar-shape crystals were obtained in different conditions containing PEG 3350, with pH ranging from 6.5 to 7.5. However, X-ray data collection from these crystals showed very low resolution and triclinic symmetry with a high-content asymmetric-unit (a.u.). Additional screening of additives identified two non-ionic detergent (*n*-dodecyl β-D-maltoside and 6-cyclohexylhexyl β-D-maltoside) that were essential to grow good-quality prismatic crystals with tetragonal symmetry and two molecules within the a.u. Crystals were grown by mixing protein solution (6 $mgml^{-1}$ in 50 mM potassium phosphate, pH 7), precipitant solution (13–18% (v/v) PEG 3350, 0.2 M sodium nitrate, 3% 2-Methyl-2,4-pentanediol, 0.1 M BisTris propane, pH 7.5),

and 5% *n*-dodecyl β-D-maltoside/6-cyclohexylhexyl β-D-maltoside, in a 1:1:0.1 protein:precipitant:detergent ratio. The complex with compound **4** was obtained by soaking crystals into precipitant solution containing 33 mM ligand for 4 h. The complex with **10** was obtained by fast soaking into precipitant solution with 10 mM ligand.

For data collection, crystals were transferred to cryoprotectant solutions consisting of mother liquor plus 25% glicerol and 5–10 mM ligand, being flash-cooled in liquid nitrogen. Diffraction data were collected using synchrotron radiation on the XALOC beamline at ALBA (Cerdanyola del Vallés, Spain). Diffraction images were processed with XDS [45] and merged using AIMLESS [46] from the CCP4 package [47]. They were indexed in the $P42_12$ space group, with two molecules in the a.u. and 66% solvent content within the unit cell. Final data collection statistics are given in Table S1 (Supplementary material).

The X-ray structure of the complexes were solved by molecular replacement using MOLREP [48] and the coordinates of native BglA (PDB code1E4I). Crystallographic refinement was performed using the programs REFMAC [49] and PHENIX [50] with flat bulk-solvent correction and local non-crystallographic symmetry (NCS). Model-building was performed with COOT [51]. For the inhibitors **4** and **10**, not present in the Protein Data Bank, a PDB model was built by MacPyMOLX11Hybrid (The PyMOL Molecular Graphics System, Version 2.0 Schrödinger, LLC). The model was used to automatically generate coordinates and molecular topologies with eLBOW [52] suitable for REFMAC refinement. The figures were generated with PyMOL.

4.5. Molecular dynamics

The molecular dynamic calculations were performed using the simple molecular dynamics module of Phenix to shake up the complex model, with the ligand position inferred from the structural superimposition of BglB (PDB code 2JIE) and KLrP (PDB code 2E9L) coordinates, respectively, onto the BglA/**4** complex. A very short molecular dynamic at 300 K was performed. The RMSD between the BglB and KLrP X-ray structures (referred to the protein backbone) and their corresponding refined complexes were 0.431 and 0.425 Å, respectively.

5. Notes

The authors declare no competing financial interest.

Acknowledgments

This work was supported by the Spanish Ministry of Economy and Competitiveness (CTQ2016-77270-R, BIO2016-76601-C3-3-R, AGL2016-75245-R), the Junta de Andalucía (FQM-345), MIUR-Italy ("Progetto Dipartimenti di Eccellenza 2018-2022" allocated to Department of Chemistry "Ugo Schiff") and Ente Cassa di Risparmio di Firenze (grant n°. 2016/0845). M. Martínez-Bailén acknowledges the Spanish government for a FPU fellowship. We thank CITIUS-University of Seville (MS and NMR facilities) and the Synchrotron Radiation Source at Alba (Barcelona, Spain) for assistance at BL13-XALOC beamline.

Appendix A. Supplementary material

Supplementary data to this article can be found online at https://doi.org/10.1016/j.bioorg.2019.103026.

References

[1] L.R. Lynd, P.J. Weimer, W.H. van Zyl, I.S. Pretorius, Microbial cellulose utilization: fundamentals and biotechnology, Microbiol. Mol. Biol. Rev. 66 (2002) 506–577.
[2] J.R. Ketudat Cairns, B. Mahong, S. Baiya, J.-S. Jeon, β-Glucosidases: multitasking, moonlighting or simply misunderstood? Plant Sci. 241 (2015) 246–259.
[3] A.H. Futerman, F.M. Platt, The metabolism of glucocerebrosides-From 1965 to the present, Mol. Genet. Metab. 120 (2017) 22–26.
[4] M. Aureli, M. Samarani, N. Loberto, G. Mancini, V. Murdica, E. Chiricozzi, A. Prinetti, R. Bassi, S. Sonnino, Current and novel aspects on the non-lysosomal β-glucosylceramidase GBA2, Neurochem. Res. 41 (2016) 210–220.
[5] L. Smith, S. Mullin, A.H.V. Schapira, Insights into the structural biology of Gaucher disease, Exp. Neurol. 298 (2017) 180–190.
[6] F.B. Bdira, M. Artola, H.S. Overkleeft, M. Ubbink, J.M. Aerts, Distinguishing the differences in β-glycosylceramidase folds, dynamics, and actions informs therapeutic uses, J. Lipid Res. 59 (2018) 2262–2276.
[7] S. He, S.G. Withers, The almond β-glucosidase is deduced to belong to family GH1 by limited sequence analysis, J. Biol. Chem. 272 (1997) 24864–24867.
[8] J. del Cueto, B.L. Møller, F. Dicenta, R. Sánchez-Pérez, β-Glucosidase activity in almond seeds, Plant Physiol. Biochem. 126 (2018) 163–172.
[9] H. Kurosu, M. Yamamoto, J.D. Clark, J.V. Pastor, A. Nandi, P. Gurnani, O.P. McGuinness, H. Chikuda, M. Yamaguchi, H. Kawaguchi, et al., Suppression of aging in mice by the hormone Klotho, Science 309 (2005) 1829–1833.
[10] G. Chen, Y. Liu, R. Goetz, L. Fu, S. Jayaraman, M.C. Hu, O.W. Moe, G. Liang, X. Li, M. Mohammadi, α-Klotho is a non-enzymatic molecular scaffold for FGF23 hormone signalling, Nature 553 (2018) 461–466.
[11] S. Lee, J. Choi, J. Mohanty, L.P. Sousa, F. Tome, E. Pardon, J. Steyaert, M.A. Lemmon, I. Lax, J. Schlessinger, Structures of β-klotho reveal a 'zip code'-like mechanism for endocrine FGF signalling, Nature 553 (2018) 501–505.
[12] Y. Hayashi, M. Ito, Klotho-related protein KLrP: structure and functions, Vitam. Horm. 101 (2016) 1–16.
[13] M. Amiri, L. Diekmann, M. von Koeckritz-Blickwede, H.Y. Naim, The diverse forms of lactose intolerance and the putative linkage to several cancers, Nutrients 7 (2015) 7209–7230.
[14] M. Behrendt, J. Polaina, H.Y. Naim, Structural hierarchy of regulatory elements in the folding and transport of an intestinal multidomain protein, J. Biol. Chem. 285 (2010) 4143–4152.
[15] J. Sanz-Aparicio, J.A. Hermoso, M. Martínez-Ripoll, J.L. Lequerica, J. Polaina, Crystal structure of β-glucosidase A from *Bacillus polymyxa*: insights into the catalytic activity in family 1 glycosyl hydrolases, J. Mol. Biol. 275 (1998) 491–502.
[16] P. Isorna, J. Polaina, L. Latorre-García, F.J. Cañada, B. González, J. Sanz-Aparicio, Crystal structures of *Paenibacillus polymyxa* β-glucosidase B complexes reveal the molecular basis of substrate specificity and give new insights into the catalytic machinery of family I glycosidases, J. Mol. Biol. 371 (2007) 1204–1218.
[17] P. Compain, A. Bodlenner, The multivalent effect in glycosidase inhibition: a new, rapidly emerging topic in glycoscience, ChemBioChem 15 (2014) 1239–1251.
[18] S.G. Gouin, Multivalent inhibitors for carbohydrate-processing enzymes: beyond the "lock-and-key" concept, Chem. Eur. J. 20 (2014) 11616–11628.
[19] N. Kanfar, E. Bartolami, R. Zelli, A. Marra, J.-Y. Winum, P. Dumy, Emerging trends in enzyme inhibition by multivalent nanoconstructs, Org. Biomol. Chem. 13 (2015) 9894–9906.
[20] C. Matassini, C. Parmeggiani, F. Cardona, A. Goti, Are enzymes sensitive to the multivalent effect? emerging evidence with glycosidases, Tetrahedron Lett. 57 (2016) 5407–5415.
[21] C. Ortiz Mellet, J.-F. Nierengarten, J.M. García Fernández, Multivalency as an action principle in multimodal lectin recognition and glycosidase inhibition: a paradigm shift driven by carbon-based glyconanomaterials, J. Mater. Chem. B 5 (2017) 6428–6436.
[22] P. Compain, Multivalent effect in glycosidase inhibition: the end of the beginning, Chem. Rec. 19 (2019), https://doi.org/10.1002/tcr.201900004.
[23] G. D'Adamio, C. Matassini, C. Parmeggiani, S. Catarzi, A. Morrone, A. Goti, P. Paoli, F. Cardona, Evidence for a multivalent effect in inhibition of sulfatases involved in lysosomal storage disorders (LSDs), RSC Adv. 6 (2016) 64847–64851.
[24] C. Matassini, C. Vanni, A. Goti, A. Morrone, M. Marradi, F. Cardona, Multimerization of DAB-1 onto Au GNPs affords new potent and selective N-acetylgalactosamine-6-sulfatase (GALNS) inhibitors, Org. Biomol. Chem. 16 (2018) 8604–8612.
[25] A. Kumar, S.M. Gaikwad, Jack bean α-mannosidase (Jbα-man): Tolerance to alkali, chelating and reducing agents and energetics of catalysis and inhibition, Int. J. Biol. Macromol. 49 (2011) 1066–1071.
[26] Y. Rivera Colón, E.K. Schutsky, A.K. Zita, S.C. Garman, The structure of human GALNS reveals the molecular basis for mucopolysaccharidosis IV A, Mol. Biol. 423 (2012) 736–751.
[27] E. Howard, A. Cousido-Siah, M.L. Lepage, J.P. Schneider, A. Bodlenner, A. Mitschler, A. Meli, I. Izzo, H.A. Álvarez, A. Podjarny, et al., Structural basis of outstanding multivalent effects in Jack Bean α-mannosidase inhibition, Angew. Chem. Int. Ed. 57 (2018) 8002–8006.
[28] A. Hottin, D.W. Wright, E. Moreno-Clavijo, A.J. Moreno-Vargas, G.J. Davies, J.-B. Behr, Exploring the divalent effect in fucosidase inhibition with stereoisomeric pyrrolidine dimers, Org. Biomol. Chem. 14 (2016) 4718–4727.
[29] E. Moreno-Clavijo, A.T. Carmona, A.J. Moreno-Vargas, L. Molina, D.W. Wright, G.J. Davies, I. Robina, Exploring a multivalent approach to α-L-fucosidase inhibition, Eur. J. Org. Chem. 7328–7336 (2013).
[30] S. Mirabella, G. D'Adamio, C. Matassini, A. Goti, S. Delgado, A. Gimeno, I. Robina, A.J. Moreno-Vargas, S. Sesták, J. Jiménez-Barbero, et al., Mechanistic insight into the binding of multivalent pyrrolidines to α-mannosidases, Chem. Eur. J. 23 (2017) 14585–14596.
[31] Y.X. Tao, P.M. Conn, Pharmacoperones as novel therapeutics for diverse protein conformational diseases, Physiol. Rev. 98 (2018) 697–725.
[32] J.-Q. Fan, A contradictory treatment for lysosomal storage disorders: inhibitors enhance mutant enzyme activity, Trends Pharmacol. Sci. 24 (2003) 355–360.
[33] C. Decroocq, D. Rodríguez-Lucena, K. Ikeda, N. Asano, P. Compain, Cyclodextrin-based iminosugar click clusters: the first examples of multivalent pharmacological chaperones for the treatment of lysosomal storage disorders, ChemBioChem 13

(2012) 661–664.
[34] A. Joosten, C. Decroocq, J. de Sousa, J.P. Schneider, E. Etamé, A. Bodlenner, T.D. Butters, P. Compain, A systematic investigation of iminosugar click clusters as pharmacological chaperones for the treatment of Gaucher disease, ChemBioChem 15 (2014) 309–319.
[35] M. Martínez-Bailén, A.T. Carmona, E. Moreno-Clavijo, I. Robina, D. Ide, A. Kato, A.J. Moreno-Vargas, Tuning of β-glucosidase and α-galactosidase inhibition by generation and *in situ* screening of a library of pyrrolidine-triazole hybrid molecules, Eur. J. Med. Chem. 138 (2017) 532–542.
[36] J. Veliks, H.M. Seifert, D.K. Frantz, J.K. Klosterman, J.-C. Tseng, A. Lindena, J.S. Siegel, Towards the molecular Borromean link with three unequal rings: double-threaded ruthenium(II) ring-in-ring complexes, Org. Chem. Front. 3 (2016) 667–672.
[37] Y.M. Chabre, C. Contino-Pépin, V. Placide, T.C. Shiao, R. Roy, Expeditive synthesis of glycodendrimer scaffolds based on versatile TRIS and mannoside derivatives, J. Org. Chem. 73 (2008) 5602–5605.
[38] M.E.C. Caines, S.M. Hancock, C.A. Tarling, T.M. Wrodnigg, R.V. Stick, A.E. Stütz, A. Vasella, S.G. Withers, N.C.J. Strynadka, The structural basis of glycosidase inhibition by five-membered iminocyclitols: the clan A glycoside hydrolase endoglycoceramidase as a model system, Angew. Chem. Int. Ed. 46 (2007) 4474–4476.
[39] R.J. Pieters, Maximizing multivalency effects in protein-carbohydrate interactions, Org. Biomol. Chem. 7 (2009) 2013–2025.
[40] Y. Hayashi, N. Okino, Y. Kakuta, T. Shikanai, M. Tani, H. Narimatsu, M. Ito, Klotho-related protein is a novel cytosolic neutral beta-glycosylceramidase, J. Biol. Chem. 282 (2007) 30889–30900.
[41] S. Tribolo, J.G. Berrin, P.A. Kroon, M. Czjzek, N. Juge, The crystal structure of human cytosolic beta-glucosidase unravels the substrate aglycone, J. Mol. Biol. 370 (2007) 964–975.
[42] G. González-Blasco, J. Sanz-Aparicio, B. González, J.A. Hermoso, J. Polaina, Directed evolution of beta -glucosidase A from Paenibacillus polymyxa to thermal resistance, J. Biol. Chem. 275 (2000) 13708–13712.
[43] M.J. Arrizubieta, J. Polaina, Increased thermal resistance and modification of the catalytic properties of a beta-glucosidase by random mutagenesis and in vitro recombination, J. Biol. Chem. 275 (2000) 28843–28848.
[44] A. Cornish-Bowden, A simple graphical method for determining the inhibition constants of mixed, uncompetitive and non-competitive inhibitors, Biochem. J. 137 (1974) 143–144.
[45] W. Kabsch, Software XDS for image rotation, recognition and crystal symmetry assignment, Acta Crystallogr. Sect. D 66 (2010) 125–132.
[46] P.R. Evans, G.N. Murshudov, How good are my data and what is the resolution? Acta Crystallogr. Sect. D 69 (2013) 1204–1214.
[47] M.D. Winn, C.C. Ballard, K.D. Cowtan, E.J. Dodson, P. Emsley, P.R. Evans, R.M. Keegan, E.B. Krissinel, A.G.W. Leslie, A. McCoy, et al., Overview of the CCP4 suite and current developments, Acta Crystallogr. Sect. D 67 (2011) 235–242.
[48] A. Vagin, A. Teplyakov, MOLREP: an automated program for molecular replacement, J. Appl. Crystallogr. 30 (1997) 1022–1025.
[49] G.N. Murshudov, A. Vagin, E.J. Dodson, Refinement of macromolecular structures by the maximum-likelihood method, Acta Crystallogr. Sect. D 53 (1997) 240–255.
[50] P.D. Adams, P.V. Afonine, G. Bunkoczi, V.B. Chen, I.W. Davis, N. Echols, J.J. Headd, L.W. Hung, G.J. Kapral, R.W. Grosse-Kunstleve, et al., PHENIX: a comprehensive python-based system for macromolecular structure solution, Acta Crystallogr. Sect. D 66 (2010) 213–221.
[51] P. Emsley, K. Cowtan, Coot: model-building tools for molecular graphics, Acta Crystallogr. Sect. D 60 (2004) 2126–2132.
[52] N.W. Moriarty, R.W. Grosse-Kunstleve, P.D. Adams, Electronic ligand builder and optimizatioN workbench (eLBOW): a tool for ligand coordinate and restraint generation, Acta Crystallog. Sect. D 65 (2009) 1074–1080.